Journal of Materials Chemistry C

Flexible-Color Tuning and White-Light Emission in Three-, Four-, and Five-component Host/Guest Co-crystals by Charge–Transfer Emissions as well as Effective Energy Transfers

Journal:	*Journal of Materials Chemistry C*
Manuscript ID	TC-ART-12-2018-006165.R1
Article Type:	Paper
Date Submitted by the Author:	08-Jan-2019
Complete List of Authors:	Ono, Toshikazu; Kyushu University, Department of Chemistry and Biochemistry Hisaeda, Yoshio; Kyushu University, Department of Chemistry and Biochemistry; Kyushu University, Center for Molecular Systems (CMS)

Journal Name

ARTICLE

Flexible-Color Tuning and White-Light Emission in Three-, Four-, and Five-component Host/Guest Co-crystals by Charge–Transfer Emissions as well as Effective Energy Transfers

Received 00th January 20xx,
Accepted 00th January 20xx

DOI: 10.1039/x0xx00000x

www.rsc.org/

Toshikazu Ono,*[a,b] Yoshio Hisaeda *[a]

Three-, four-, and five-component host/guest crystals with multi-color and white light emission is described. Our strategy is based on confinement of aromatic donor guests in supramolecular acceptor hosts. The supramolecular acceptor hosts (NDI–TPFB) were composed of *N,N'*-dipyrid-3-yl-1,4,5,8-naphthalenediimide (NDI) with two tris(pentafluorophenyl)borane (TPFB) linked by boron–nitrogen dative bonds as Lewis acid–base pairs, which spontaneously formed upon mixing the components. In the first part, a set of three-component crystals with 14 different aromatic guests were characterized to elucidate the structure–property relationships. In the latter part, a series of 17 types of four- and five-component crystals were formed with the use of binary or ternary guest inclusion systems, and their structural and photophysical properties were investigated. Among them, 14 types of crystals were formed effectively without destroying the crystal structure, as determined by X-ray diffraction and fluorescence microscope. Notably, flexible color tuning, including white light emission, was realized by tuning the guest ratio and the combinations. Various intermolecular interactions such as C–H•••F interactions, π-π stacking, charge-transfer interactions, and inclusion phenomena were important to forming the crystals. This approach yields a rational solution of multicomponent crystals could be potentially useful for obtaining novel photofunctional solid-state systems.

Introduction

The investigation of co-crystals or multicomponent crystals have been drawing increasing attention owing to their potential for applications as pharmaceuticals in addition to advanced optical, electrical, and magnetic materials.[1-5] This is due to the individual molecules have their own unique characteristics but hidden properties can be revealed when they are hybridized with other molecules.[6, 7] One example is an organic solid-state emissive material for which flexible color tuning has been achieved.[8-20] Recent advances in supramolecular solid-state chemistry (crystal engineering) have considerably enhanced our understanding of molecular recognition and intermolecular interactions leading to the formation of multicomponent crystals. Typically, noncovalent interactions including hydrogen bonds, halogen bonds, C-H– π interactions, $\pi-\pi$ stacking, charge–transfer (CT) interactions, ion-pairs, and inclusion phenomena and their combinations have been used widely to direct supramolecular co-crystal formation. [21-26] For example, Yang and co-workers have reported systematic color tuning of 1,4-bis(4-cyanostylryl)benzene by a co-crystallization method with halogen- and hydrogen-bonds.[8] Dong, Hu and co-workers have reported rational design of optoelectronic co-crystals by halogen-bond and CT interactions. [12] Kim and co-workers have reported a "direct heavy atom effect" principle for the design and synthesis of color tunable organic phosphors.[9] Nishida and co-workers have reported the delayed photoluminescence properties of phthalimide co-crystals.[13] However, except for notable contributions,[27-36] most studies on organic co-crystals led to the formation of binary organic solids. Examples of ternary combinations of different molecules are comparatively rare. Conversely, metal alloys, inorganic compounds, and metal-organic frameworks (MOFs) or porous coordination polymers (PCPs) readily form multicomponent solids in the form of solid solutions. [5, 37-39] However, creating multicomponent crystals of purely organic molecules remains challenging.[40] Organic molecules possess a wide variety of sizes, intricate shapes and complicated weak intermolecular interactions. Hence, slight modifications of the molecular structures often induce phase segregation and inhibit their co-assembly. Therefore, crystals are not so easily tuned as amorphous materials, and effective co-crystallization of organic components is deemed to be difficult. Up to now, there is nearly no reports on multicomponent crystals with a desired crystal structure and optical properties. Systematic color-tuning of multicomponent crystals, including multi-color emission such as white-light emission, remains a challenging task. Design of white light emitting materials is not straightforward. Mixing of multiple emitting materials is rarely successful due to the negative effect

[a] Department of Chemistry and Biochemistry, Graduate School of Engineering, Center for Molecular Systems (CMS), Kyushu University, Fukuoka 819-0395, Japan
[b] PRESTO, Japan Science and Technology Agency (JST), 4-1-8 Honcho, Kawaguchi, Saitama 332-0012, Japan
*Email - tono@mail.cstm.kyushu-u.ac.jp

†Electronic Supplementary Information (ESI) available: Details of experimental procedures, spectroscopic data. See DOI: 10.1039/x0xx00000x

of the intermolecular interaction and the energy transfer process. Recently, Lee, Liao and co-workers have reported the white-light emitting CT microtubes by incorporating a dopant of pyrene into blue-emitting naphthalene-1,2,4,5-tetracyanobenzene (TCNB) matrix.[14] Similarly, tunable emission was also achieved by co-crystallization of aromatic molecules involving TCNB.[15] Exploration of design and control of multicomponent crystals should allow functions of the organic molecules to be accumulated by the same strategy as employed with inorganic materials and metal-organic hybrid materials.

To address these challenges, we have recently reported naphthalenediimide-based host–guest crystals that showed multicolor photoluminescence by accommodating aromatic guest molecules.[19] These ternary systems consisted of supramolecular-hosts (NDI–TPFB complexes), *N,N'*-dipyrid-3-yl-1,4,5,8-naphthalenediimide (NDI) with two tris(pentafluorophenyl)borane (TPFB) linked by boron–nitrogen dative bonds as Lewis acid-base pairs, and aromatic molecules as the guest (Guest). In a preliminary report, we showed single-crystal X-ray structure analyses and photophysical properties of three-component crystals with seven aromatic guests. This design allowed electron deficient NDI and electron rich aromatic guest molecules to interact intimately through CT interactions in the crystals. This combination resulted in guest-dependent fluorescence emission from deep blue-to-orange (450–600 nm) depending on the ionization potential (IP) of the aromatic guest molecules. In contrast to aggregation-induced quenching, these luminescent materials are non-emissive in dilute solution, but become highly emissive in the solid state and can be regarded as a type of aggregation-induced emission enhancement. [41]

On the basis of these early results, we were motivated to apply this strategy to a broader range of guests to test the generality of the preparation of three-component crystals. Second, we wished to extend the strategy to test whether four- and five-component crystalline materials could be prepared in a predictable way. Third, we wished to tune the desirable solid-state fluorescence emission from deep blue-to-near infrared (NIR) region and generate white-light under UV light excitation by a crystal engineering approach. White light emission is particularly useful for practical applications of organic solid-state lighting sources and in full-color displays, sensor materials, and supramolecular chemistry contribute to this field. [14, 42-50]

Here, we describe a supramolecular approach for the systematic preparation of three-, four-, and five-component crystals consisting of supramolecular acceptor-hosts (NDI–TPFB complexes) and various aromatic guests and their combinations as shown in Fig. 1. In this article, we report on a set of three-component crystals with 14 different aromatic guests (**1**–**14**) and full characterization of single crystal structures by X-ray diffraction, and their color-tunable photophysical properties in the crystals. In the later part, systematic preparation of a set of 14 types of four- and five-component crystals through the use of binary or ternary guest inclusion systems, and their structural and photophysical properties were investigated. Naphthalene diimide is one of the most studied compounds in the fields of supramolecular chemistry, catalysis, and sensors. [51-64] We believe that the present study suggests a rational solution to multicomponent crystals for obtaining novel photofunctional solid-state systems.

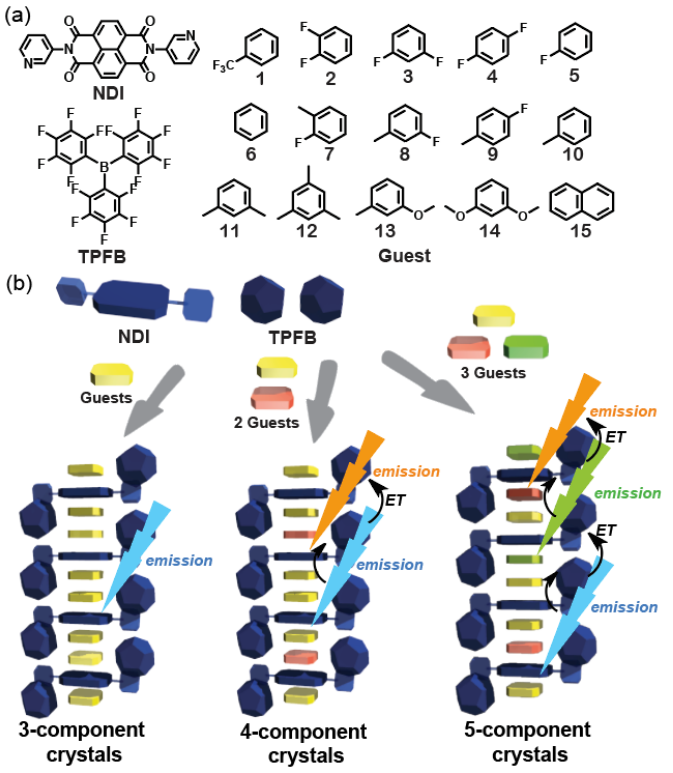

Fig. 1 (a) Chemical Structure of the multicomponent crystal motif used in this study. (b) Schematic illustration of three-, four-, and five-component crystalline materials.

Results and Discussion

Three-component Crystals

We selected 14 representative small aromatic molecules (**1**–**14**), which lacked visible fluorescence, to be the guests for preparation of three-component crystals. The guest molecules were benzene derivatives with different substituents, ranging from strongly electron-withdrawing to strongly electron-donating groups, and all were liquids at room temperature. The structural features of all the three-component crystals were successfully examined by single-crystal X-ray structure analyses, and could be divided into 3 groups based on the crystal system. Notably, multicomponent crystals obtained in this work were stable in air for at least 1 year at room temperature. These properties reveal not only the rigidity of the crystals but also the promise that these crystals have in for real applications.

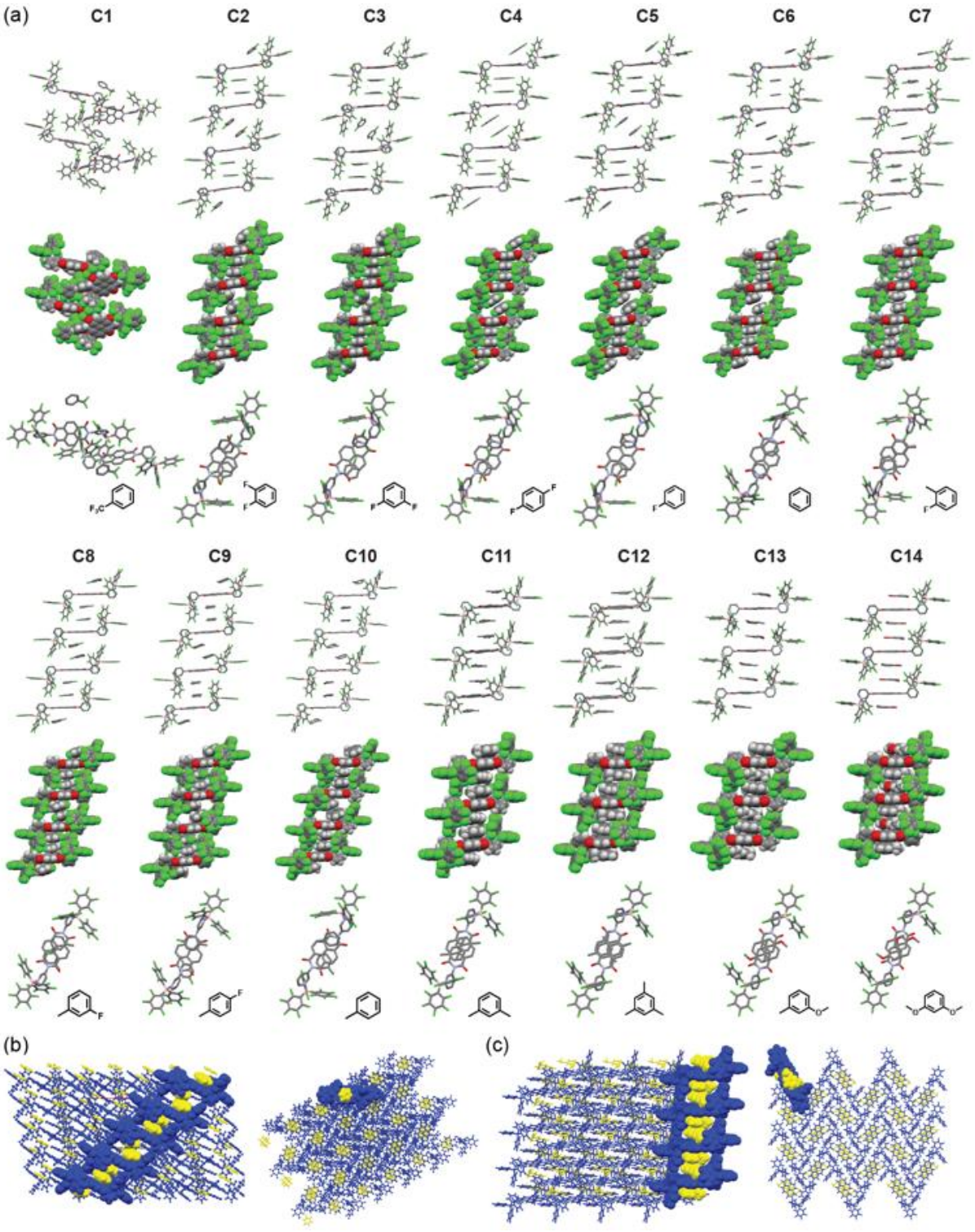

Fig. 2 Crystal structure of **C1–C14**, illustrated as a blend of tubular and space-filling representations. The crystal (**C1**) is composed of NDI, TPFB, and (trifluoromethyl)benzene (**1**) in a 1:2:1 molar ratio. The other crystals (**C2**–**C14**) are composed of NDI, TPFB, and guest in a 1:2:2 molar ratios. The top and center panels depict side views. The bottom panels depict top-view. In the top and bottom panels are illustrated as tubular representation, but hydrogen atoms are omitted for the sake of clarity. The center panels are illustrated as space-filling representation. Color code: C, gray; H, white; O, red; N, purple; B, pink; F, green. (b) Crystal packing of **C6**, and (c) **C12**. The color changed to show the supramolecular acceptor host (blue) and donor guest (yellow).

Table 1 Photophysical properties of **C1**–**C14**.

No.	Guest molecule	IP of guest (eV)[a]	$\lambda_{max,em}$ (nm)	PLQY (%)[b]	λ_{av} (ns)[c]	K_r (s^{-1})[d]	K_{nr} (s^{-1})[d]	CIE1931 (x,y)
C1	**1,** (trifluoromethyl)benzene	9.69	412	1.1	<0.1	-	-	(0.224, 0.222)
C2	**2,** *o*-difluorobenzene	9.29	420	3.0	1.3	2.3×10^7	7.5×10^8	(0.241, 0.280)
C3	**3,** *m*-difluorobenzene	9.33	420	7.9	1.6	4.9×10^7	5.8×10^8	(0.254, 0.353)
C4	**4,** *p*-difluorobenzene	9.16	424	4.0	2.5	1.6×10^7	3.8×10^8	(0.248, 0.279)
C5	**5,** fluorobenzene	9.20	448	7.9	5.4	1.5×10^7	1.7×10^8	(0.195, 0.209)
C6	**6,** benzene	9.24	450	16.7	6.6	2.5×10^7	1.3×10^8	(0.176, 0.154)
C7	**7,** *o*-fluorotoluene	8.92	460	18.9	11.8	1.6×10^7	6.9×10^7	(0.178, 0.210)
C8	**8,** *m*-fluorotoluene	8.91	466	28.3	14.0	2.0×10^7	5.1×10^7	(0.171, 0.219)
C9	**9,** *p*-fluorotoluene	8.79	480	6.8	14.1	4.8×10^6	6.6×10^7	(0.262, 0.370)
C10	**10,** toluene	8.83	472	17.3	14.1	6.9×10^6	3.3×10^7	(0.219, 0.364)
C11	**11,** *m*-xylene	8.56	509	26.2	24.9	1.8×10^7	5.1×10^7	(0.282, 0.538)
C12	**12,** mesitylene	8.40	531	10.8	14.5	2.6×10^7	2.1×10^8	(0.402, 0.562)
C13	**13,** *m*-methylanisole	8.10	600	1.5	4.2	3.8×10^7	2.5×10^9	(0.557, 0.436)
C14	**14,** 1,3-dimethoxybenzene	8.00	631	<1	0.4	-	-	(0.565, 0.362)

[a] The ionization potential (IP) values were taken from refs 70 and 71. [b] Absolute photoluminescence quantum yields (PLQY) were determined using a calibrated integrating sphere system with excitation at 370 nm. [c] The fluorescence lifetime values of **C1–C14** in the crystalline state were measured at their emission peaks with excitation at 365 nm. [d] $k_r=PLQY/\tau_{av}$, $k_{nr}=(1-PLQY)/\tau_{av}$

The multicomponent crystal design element consisted of three major components: (i) boron-nitrogen (B–N) dative bonding between Lewis acid-base pairs,[65] which formed a predictable supramolecular acceptor host (NDI–TPFB complex) (ii) aromatic donor–acceptor (D–A) interactions between electron-rich aromatic guests and, electron-deficient NDI, and (iii) inclusion phenomena, which promoted self-assembly/co-crystallization processes. Notably, this strategy used an intrinsically rigid supramolecular acceptor-host (NDI–TPFB complex) to achieve effective molecular recognition and to host the various types of aromatic guests. Here we discuss the crystal structures and the intermolecular interactions including previously reported structures of **C1**, **C5**, **C6**, **C8**, and **C10**–**C13**. [19] [62]

Crystal Structure of C1

Three-component crystals of **C1** consisted of NDI, two TPFBs and one (trifluoromethyl)benzene molecule, which crystallized in the triclinic space group P-1 (Fig. 2a). In the NDI–TPFB complex, the lengths of the B–N dative bonds between the pyridyl moiɔety of NDI and TPFB were 1.631 and 1.637 Å, as determined from the crystal structure. The formation of mutually interdigitated dimeric structures of NDI–TPFB complexes was observed in the crystals, and one (trifluoromethyl)benzene molecule was located in the void space of the crystals. Judging from the crystal structure, there were no CT interactions between NDI and (trifluoromethyl)benzene as a guest in the crystal. It seems that (trifluoromethyl)benzene lacked sufficient donor ability to interact with NDI. Hirshfeld surface analysis was also performed for visualizing and quantifying intermolecular interactions in the crystals. The result clearly showed that C–H•••F interactions[66] (2.138 Å) and C–H•••O interactions[67] (2.267 Å) were observed in the crystal structure, which may contribute to the crystal formation (Fig. S5).

Crystal Structures of C2–**C9**

Three-component crystals **C2**–**C9** consisted of NDI, two TPFBs and two guest molecules, which crystalized in the monoclinic space group $P2_1/c$ (Fig. 2a, 2b). It is clear that the NDI–TPFB complex formed a one-dimensional (1D) column structure, which accommodated two guest molecules inside the cavity. The bulky substituents of TPFB contributed to the formation of an inclusion space associated with steric hindrance.[25] The guests in the crystals were organized by (i) a face-to-face fashion with the electron-deficient NDI, wherein the guest and NDI components were separated by c.a. 3.5–3.6 Å, and (ii) by location in the cavity to fill the space. It is likely that CT interactions between aromatic guests and NDI were formed in former case, which might contribute to the formation of one-dimensional crystal lattice structures. For example, **C8** is a three-component crystal in which *m*-fluorotoluene (**8**) is included as a guest molecule. The supramolecular host NDI–TPFB was connected through a B–N dative bond (1.626 Å and 1.640 Å). Hirshfeld surface analysis revealed that a significant contribution of C–H•••F interactions between the *m*-fluorotoluene and TPFB (2.382 Å) and TPFB and pyridyl moiety of NDI (2.178 Å) was observed in the structure (Fig. S5). These multiple intermolecular interactions should stabilize the formation of multicomponent crystals.

Crystal Structure of C10–**C14**

Three-component crystals **C10–C14** consisted of NDI, two TPFBs and two guest molecules, which crystalized in the monoclinic

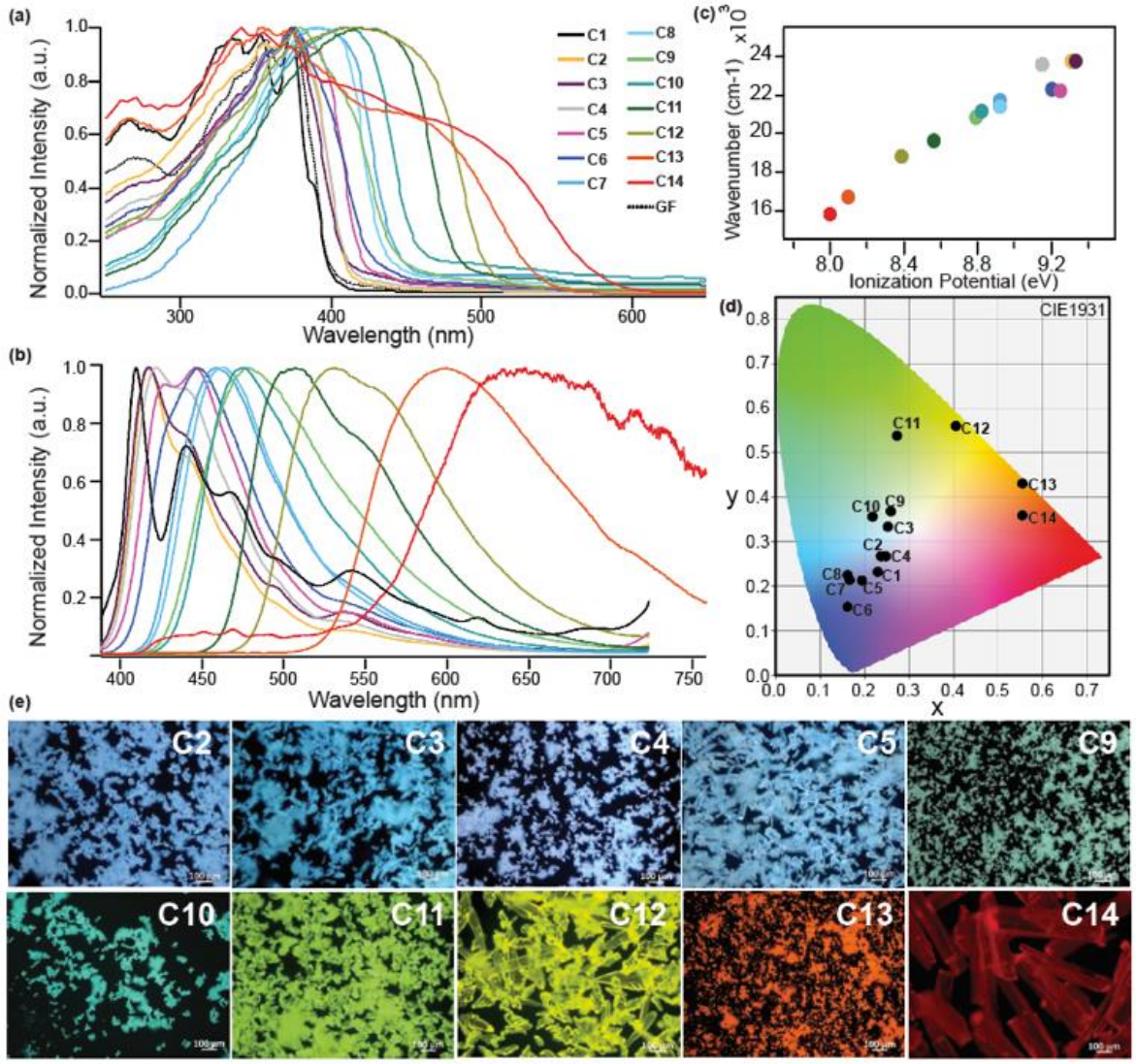

Fig. 3 (a) Height normalized UV-vis diffuse-reflectance spectra of **C1–C14** and a guest-free crystal (**GF**). (b) Height normalized emission spectra of **C1–C14.** Excitation at 370 nm. (c) Relationship between the emission energies of the crystals (**C2–C14**) and the ionization potential (IP) of the guest molecules (**2–14**). The linear correlation implies that the CT complexation dominates the emission energies. (d) Emission colors in the CIE 1931 chromaticity diagram of **C1–C14**. (e) Fluorescence microscopy images of **C2**, **C3**, **C4**, **C5**, **C9**, **C10**, **C11**, **C12**, **C13**, and **C14**. Excitation at 330–380 nm, emission at >420 nm.

space group $P2_1/n$ (Fig. 2a, 2c). Supramolecular complexes formed between one NDI and two TPFBs linked by B–N dative bonds as Lewis acid-base pairs in all the crystals. The three C_6F_5 substituents of TPFB were arranged in a propeller-like fashion and acted as bulky substituents, enabling the accommodation of two guest molecules sandwiching the NDI moiety in a face-to-face manner. It is likely that the guest with the higher donor ability formed strong CT interactions, which promoted the self-assembly/cocrystallization processes to form a one-dimensional crystal lattice. These crystals also contain multiple C–H•••F interactions in the solid-state (Fig. S5).

Thermogravimetry of Three-component Crystals

Thermogravimetric analysis (TGA) was used to determine the guest inclusion and thermostability of the three-component crystals. TGA results of **C1–C14** are plotted in the temperature range of 30 to 500°C, as shown in Fig. S6–S8. TGA results of NDI, TPFB, and guest free crystal (**GF**) are also plotted in the temperature range from 30 to 500°C as reference compounds (Fig. S9). These results suggest that the NDI decomposed in the range of 350 to 460°C, TPFB sublimated in the temperature range of 100 to 200°C, and **GF** decomposed in the temperature range of 250 to 350°C. **GF** showed different thermal durability from those of both NDI and TPFB itself, suggesting that **GF** formed a supramolecular acceptor host (NDI–TPFB complex) by boron-nitrogen (B–N) dative bonding between the Lewis acid–base pairs in the solid state. The TGA results confirmed that the crystal (**C1**) was composed of NDI, TPFB, and (trifluoromethyl)benzene in a 1:2:1 molar ratio. The thermogram of **C1** revealed two stages: the first weight loss at a temperature range from 80 to 120°C corresponded to the evaporation of one (trifluoromethyl)benzene, and the second stage was the subsequent weight loss after 300°C corresponding to the loss of the supramolecular acceptor host

(NDI–TPFB complex) itself. The TGA results confirmed that **C2–C14** was composed of NDI, TPFB, and the guest in a 1:2:2 molar ratio. For example, in the case of **C8**, the first weight loss at a temperature range from 120 to 160°C corresponded to the evaporation of two *m*-fluorotoluene, and the second stage represents subsequent weight loss after 300°C owing to the weight loss of the supramolecular acceptor host (NDI–TPFB complex). Moreover, in the case of **C14**, the first weight loss at a temperature range from 160 to 220°C corresponds to evaporation of two 1,3-dimethoxybenzene, and the second stage was the subsequent weight loss after 300°C owing to weight loss of loss of the supramolecular acceptor host (NDI–TPFB complex). The first weight loss depends on the thermostability of the three-component crystals (**C1–C14**), which essentially reflects the type of guest molecules. Elemental analyses further supported the formation of three-component crystals (Table S1).

Steady-State Absorption and Fluorescence Spectroscopy of Three-component Crystals

The photophysical properties of the three-component crystals **C1–C14** highlight the uniqueness of the compounds. We conducted UV-vis diffuse-reflectance spectroscopy measurements of the **C1–C14** and **GF** using an integrating sphere, as shown in Fig. 3a. Although **GF** and **C1** showed similar absorption spectra, **C2–C14** showed a new absorption band in the visible region from 400 to 600 nm, which depended on the included guest molecules. The positions of the absorption band red-shifted as the electron donating strength of the guest molecule increased. This result can be attributed to the formation of an intermolecular CT complex between the electron deficient NDI and electron rich guest molecules in the ground state. The CT band of our system was much higher than those previous reported for a naphthalenediimide-aromatic molecule system in the solution phase[68] or inside porous coordination polymers.[69] Thus, the highly-ordered arrangement of the **NDI** and guest in the crystals might contribute to the strong CT absorption in the ground state.

The three-component crystals (**C1**–**C14**) also showed unique photoluminescence characteristics, which reflected the type of guest molecule. Fluorescence microscope images based on light-emission from the three crystals are shown in Fig. 3e. Under UV light irradiation at 370 nm, color variation over the range electron-deficient guests such as difluorobenzene (**C2–C4**), from visible-to-NIR luminescence was achieved (Fig. 3b). The CIE (*x*,*y*) 1931 chromaticity coordinates were calculated from the emission spectra and the plots are summarized (Fig. 3d). When fluorobenzene (**C5**) or benzene (**C6**) were selected as guest molecules, blue light emission was observed. In the case of fluorotoluene (**C7–C9**) or toluene (**C10**) guest molecules, cyan emission was observed. For more electron-rich aromatic guests such as *m*-xylene (**C11**), mesitylene (**C12**), *m*-methylanisole (**C13**), or 1,3-dimethoxybenzene (**C14**), green (λ_{max} = 531 nm), yellow-green (λ_{max} = 531 nm), orange (λ_{max} = 600 nm), or red (λ_{max} = 631 nm) to near infrared (NIR) broad-emission was observed. Notably the emission occurred with high quantum yields (Φ_{PL}) of 16.7% for **C6**, 18.9% for **C7**, 28.3% for **C8**, 17.3% for **C10**, 26.2% for **C11**, 10.8% for **C12**, in the crystalline state. This result can most likely be attributed to the crystal structure and the electronic properties of the guest molecules. In contrast, the strong electron-donating properties of *m*-methylanisole (IP = 8.10 eV) and 1,3-dimethoxybenene (IP = 8.00 eV) might quench the CT based photoluminescence through the contribution of a radical ion pair state, in which the total electron transfer from *m*-methylanisole and 1,3-dimethoxybenzene to NDI deactivates the excited state by non-radiative decay. Therefore, low quantum yields (Φ_{PL}) of 1.5% for **C13** and < 1% for **C14** were observed. Owing to the weak contribution to the photoluminescence properties from the CT state of **C14**, NDI-based emission (400–500 nm) was monitored in the spectra.

These practically important photoluminescence properties of the multicomponent crystals can be ascribed to the host–guest interactions between NDI and guest molecules in the crystals. The emission of **C1** yielded weak blue emission (Φ_{PL} = 1.1%) under UV light irradiation, which likely originates from NDI itself. The relationship between the emission energy maxima of the multicomponent crystal (**C2**–**C14**) and the IP of the guest molecules[70, 71] is shown in Fig. 3c. The linear correlation indicates that the ground state CT complexation between NDI and the guest dominates the photoluminescence in the crystals.

Fluorescence Lifetime Measurements of Three-component Crystals.

To obtain additional information on the emissive species and photophysical processes involved, the profiles were measured and the corresponding emission decay curves are shown in Fig. S25 and Fig. S26. The results were summarized in Table S1. When an electron-deficient guest, such as difluorobenzene (**C2–C4**), fluorobenzene (**C5**) or benzene (**C6**), was selected as a guest molecule, the average lifetimes (λ_{av}) were in the range of 1.3–6.6 ns. When fluorotoluene (**C7–C9**), toluene (**C10**), *m*-xylene (**C11**), or mesitylene (**C12**) was selected as a guest molecule, relatively long average lifetimes (λ_{av}) were observed in the range of 11.8–24.9 ns. Conversely, strong donating guests such as *m*-methylanisole (**C13**) and 1,3-dimethoxybenene (**C14**) showed shorter average lifetimes (λ_{av}) of 4.2 and 0.4 ns. These results indicated that the photoluminescence of **C2–C14** derived from fluorescence emission resulting from excited CT states between NDI and guest molecules in the crystals. The radiative (K_r) and non-radiative (K_{nr}) rate constant of **C2–C13** were calculated, which supported the fact that their photophysical properties were influenced by guest inclusion (Table 1). The average lifetime of **C1** was less than 0.1 ns. This result is supported by the fact that blue emission of **C1** should originate from NDI itself.

Table 2 Photophysical Properties of **MC1**–**MC14** in the Crystalline State

No.	Molar ratio of included guests [a]	λ_{max} (nm)	Φ_{PL} [b] (%)	CIE1931 (x,y)
MC1	**8/15** (97.8/2.2)	466	24.5	(0.235, 0.282)
MC2	**8/15** (97.3/2.7)	466, 548	25.3	(0.279, 0.320)
MC3	**8/15** (96.7/3.3)	466, 556	19.5	(0.332, 0.373)
MC4	**8/15** (95.3/4.7)	466, 562	18.4	(0.361, 0.394)
MC5	**8/15** (91.3/8.7)	466, 567	17.0	(0.440, 0.458)
MC6	**10/15** (93.5/6.5)	478, 560	16.5	(0.286, 0.394)
MC7	**10/15** (92.0/8.0)	478, 552	13.2	(0.342, 0.422)
MC8	**10/15** (87.9/12.1)	478, 567	11.1	(0.421, 0.457)
MC9	**11/15** (94.8/5.2)	526	16.0	(0.336, 0.526)
MC10	**11/15** (93.9/6.1)	545	11.9	(0.383, 0.528)
MC11	**11/15** (90.8/9.2)	555	14.1	(0.419, 0.519)
MC12	**8/11/15** (89.2/9.1/1.7)	491	23.7	(0.272, 0.437)
MC13	**8/11/15** (86.3/12.5/2.1)	513	18.1	(0.332, 0.490)
MC14	**8/11/15** (81.0/14.5/4.5)	548	17.6	(0.368, 0.485)

[a] Values in parentheses correspond to ratio of guests determined by ^{1}H NMR spectra [b] Absolute photoluminescence quantum yields (Φ_{PL}) were determined using a calibrated integrating sphere system with excitation at 370 nm.

Four-, and Five-component Crystals

The above successful findings motivated us to investigate if the supramolecular acceptor host (NDI–TPFB complex) could accommodate multiple guests. Multiple guest systems would allow flexible photo-functional design to be realized by crystal engineering approaches. For example, multi-color and white-light emitting organic solid state materials have attracted considerable interest in recent years. However, in terms of research of mixed crystals of purely organic materials, it is extremely difficult to prepare multicomponent crystals and solid-solutions composed of four, five, or more components. Here we demonstrated a series of 14 types of four- and five-component crystals with flexible color-tuning and white-light emitting organic solid state crystalline materials through the combination of two-component supramolecular acceptor hosts (NDI–TPFB complexes) and binary or ternary guest inclusion systems. The basic concept of this study is illustrated in Fig. 1(b). The experimental details are discussed below.

Inclusion Abilities and Solid-state Structures of Four-, and Five-component Crystals (MC1–**MC14)**

Among various binary combinations of guests for preparing four-component solid-solution systems, our first trial was to prepare white-light emitting materials by mixing of *m*-fluorotoluene and *m*-methylanisole as a binary guest. We predicted that white light emission could be obtained by combining cyan and orange emission, from the cyan light emitting crystals **C8** (*m*-fluorotoluene) and the orange light emitting crystals **C13** (*m*-methylanisole). Unfortunately, however, the obtained crystals were not homogeneously guest-distributed crystals (**MC15**–**MC17**), which was estimated from fluorescence microscope images (Fig. S28). Moreover, the quantum yields (Φ_{PL}) were rather low, namely 2.5% for **MC15**, 2.2% for **MC16**, and 0.9% for **MC17**; however, **MC16** showed white-light emission by emission spectra (Fig. S29). Therefore, we considered that the luminescent colors of these materials were controlled by the IP of the guest molecules. The use of naphthalene (IP = 8.12 eV) as a guest molecule instead of *m*-methylanisole (IP = 8.10 eV) gave good results, although three-component crystals of **C15** consisted of NDI, TPFB and naphthalene (**15**) are not obtained at this stage. A set of four-component crystals composed of supramolecular acceptor-host NDI–TPFB complexes were prepared as a binary host including: *m*-fluorotoluene/naphthalene as a binary guest (**MC1–MC5**), toluene/naphthalene as a binary guest (**MC6**–**MC8)**, *m*-xylene/naphthalene as a binary guest (**MC9**–**MC11**). Moreover, a set of five-component crystals composed of supramolecular the acceptor-host (NDI–TPFB complex) as a binary host including: *m*-fluorotoluene/*m*-xylene/naphthalene as a ternary guest (**MC12**–**MC14)**, were prepared. The molar ratios of the multicomponent crystals (**MC1**–**MC14**) were confirmed by ^{1}H NMR (Fig. S14–S17) and the results are summarized in Table 2. These results suggested that the molar ratio of the binary- or ternary- component guest systems was regulated by the experimental conditions. TGA of the multicomponent crystals supported the inclusion of the guest molecules and formation of supramolecular acceptor host (NDI–TPFB complex), which corresponded to a decomposition temperature in the temperature range of 250 to 350 °C (Fig. S10–S13). Moreover, Powder X-Ray diffraction (PXRD) patterns of the multicomponent crystals including *m*-fluorotoluene/naphthalene as a binary guest (**MC1**–**MC5**), toluene/naphthalene as a binary guest (**MC6**–**MC8)**, *m*-xylene/naphthalene as a binary guest (**MC9**–**MC11**), and *m*-fluorotoluene/*m*-xylene/naphthalene as a ternary guest

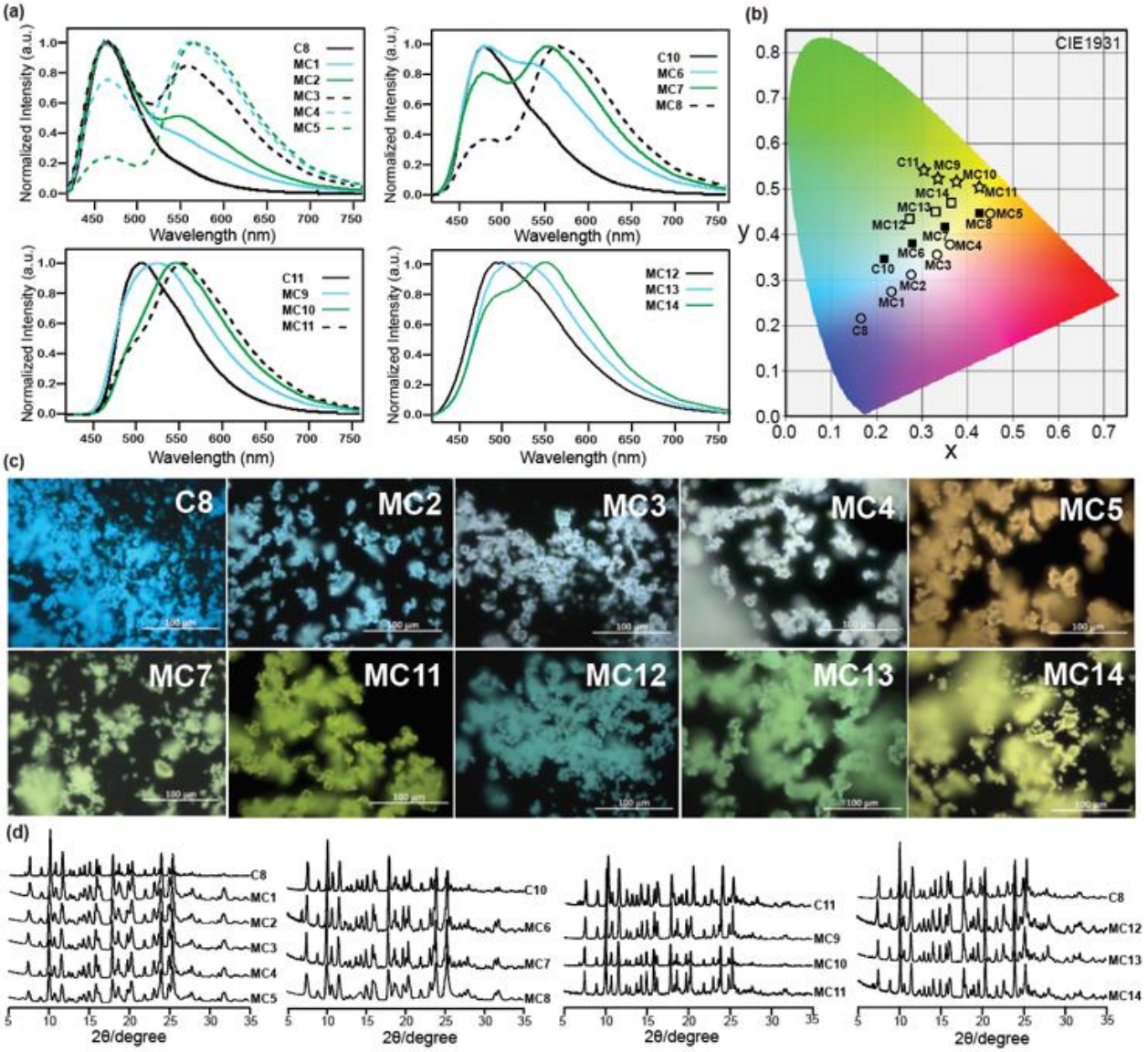

Fig. 4 (a) Height-normalized emission spectra of three- (**C8**, **C11**, **C12**), four- (**MC1**–**MC11**), and five-component crystals (**MC12**–**MC14**). Excitation at 370 nm. (b) Emission colors in the CIE 1931 chromaticity diagram of **C8**, **C11**, **C12**, and **MC1**–**MC14**. (c) Fluorescence microscopy images of **C8**, **MC2**, **MC3**, **MC4**, **MC5**, **MC7**, **MC11**, **MC12**, **MC13**, and **MC14**. Excitation at 330–380 nm. Emission at >420nm. (d) Powder X-Ray diffraction (PXRD) pattern of multicomponent crystals. (a) **C8** and **MC1**–**MC5**, (b) **C11** and **MC6**–**MC8**, (c) **C12** and **MC9**-**MC11**, and (d) **C8** and **MC12**–**MC14**.

(**MC12**–**MC14)**, agreed well with those of the corresponding single-guest, monoclinic bulk crystals [Fig. 4(d)]. Notably, the addition of multiple guests did not disrupt the original crystal structures. We can infer that the inclusion of two and three guests in the supramolecular-acceptor host (NDI–TPFB complex) did not induce phase segregation in these multicomponent crystalline systems. The multicomponent crystals were stable in air for at least 1 year at room temperature.

Steady-State Absorption and Fluorescence Spectroscopy of Five-, and Four-component Crystals (MC1–**MC14**)

The photophysical properties of the four- and five-component crystals **MC1**–**MC14** highlight the unique features of these compounds. We measured the UV-vis diffuse-reflectance spectra of **MC1**–**MC14** using an integrating sphere, and the results are shown in Fig. S21–S24. The four-component crystals **MC1**–**MC5** showed similar absorption profiles to those of the corresponding crystal (**C8**), **MC6**–**MC8** also showed a similar spectral shape to the corresponding crystal (**C11**), and **MC9**–**MC11** showed a similar spectra shape to the corresponding crystal (**C12**). The five-component crystals **MC12**–**MC14** showed similar spectra shape to the corresponding crystal **C8**. Considering the binary and ternary guest composition ratios confined in the multicomponent crystalline systems (**MC1**–**MC14**), the absorption spectra might be expected to be influenced by the majority of guests. The emission properties of *m*-fluorotoluene/naphthalene binary guest systems **MC1**–**MC5** yielded cyan (466 nm) and yellow-orange (c.a. 560 nm) emission [Fig. 4(a)]. White light emission was observed for **MC2** [λ_{max} = 466 and 548 nm; CIE 1931 color coordinates: (0.279, 0.320)], **MC3** [λ_{max} = 466 and 556 nm; CIE 1931 color coordinates:

(0.332, 0.373)], and **MC4** (λ_{max} = 466 and 562 nm; CIE 1931 color coordinates: (0.340, 0.375)). Notably, these emissions were close to ideal white light emission CIE 1931 color coordinates (0.33, 0.33). Obviously, under excitation by UV light, uniform white light was emitted from the crystals. As described above, the molar ratio of *m*-fluorotoluene/naphthalene was 97.8/2.2 for **MC1**, 96.7/3.3 for **MC2**, 96.3/3.7 for **MC3**, 95.9/4.1 for **MC4**, and 91.3/8.7 for **MC5**, as determined by ^{1}H NMR. These results strongly suggest that the photoluminescence colors could be tuned by adjusting the guest inclusion ratios. Additionally, relatively high photoluminescence quantum yields (Φ_{PL}) were exhibited: Φ_{PL} = 24.5% for **MC1**, Φ_{PL} = 25.3% for **MC2,** Φ_{PL} = 19.5% for **MC3**, Φ_{PL} = 18.4% for **MC4**, and Φ_{PL} = 17.0% for **MC5** in the crystalline state. Combined with the above mentioned PXRD results, these results clearly indicate that *m*-fluorotoluene/naphthalene binary guest systems were randomly and homogeneously dispersed into supramolecular-acceptor hosts (NDI–TPFB complex), and the unique color-tuning and white light emission originated from excited electronic CT states as well as effective energy transfer in the crystals. In addition, when the above emission spectra were transformed to CIE 1931 chromaticity coordinates, we confirmed that the emission color of the *m*-fluorotoluene/naphthalene binary guest systems derive from color mixing of cyan and yellow at different guest ratios [Fig. 4(b)]. A nearly straight line could be drawn across all points of CIE chromaticity coordinates, from point **C8** (0.171, 0.219), **MC1** (0.235, 0.282) to point **MC5** (0.440, 0.457) in the CIE 1931 chromaticity space. The above straight line also crossed the white region. Therefore, it is possible to tune the emission color to white light by simply changing *m*-fluorotoluene/naphthalene binary guest systems: **MC2** (0.279, 0.320), **MC3** (0.332, 0.373) and **MC4** (0.340, 0.375) in the CIE 1931 chromaticity diagram. This concept might enable the preparation of multicomponent crystals in which luminescent colors are easily mixed by selecting and combining guest molecules. Toluene/naphthalene binary guest systems (**MC6**–**MC8**), and *m*-xylene/naphthalene binary guest systems (**MC9**–**MC11**) show that color tuning of different luminescent materials is possible, as shown in the CIE 1931 chromaticity coordinates, by optimization of the mixing ratio of guests. Furthermore, five-component crystals were successfully prepared by mixing *m*-fluorotoluene/*m*-xylene/naphthalene ternary guest systems (**MC12**–**MC14**). Different luminescent crystalline materials were obtained, as shown by optimal mixing of guests such as green-blue for **MC12** [λ_{max} = 466 nm, 548 nm; CIE 1931 color coordinates: (0.279, 0.320)], green-yellow for **MC13** [λ_{max} = 466 and 548 nm; CIE 1931 color coordinates: (0.279, 0.320)] and yellow **MC14** [λ_{max} = 466 nm, 548 nm; CIE 1931 color coordinates: (0.279, 0.320)] light emission. Additionally, relatively high photoluminescence quantum yields (Φ_{PL}) were exhibited including 23.7% for **MC12**, 18.1% for **MC13,** and 17.6% for **MC14** in the crystalline state. These results suggest that appropriate guest selection and combination could enable further optimization of the emission color of multicomponent crystalline systems. Notably, preparation of multicomponent crystals in this work showed quite-high reproducibility and repeatability under the same experimental conditions.

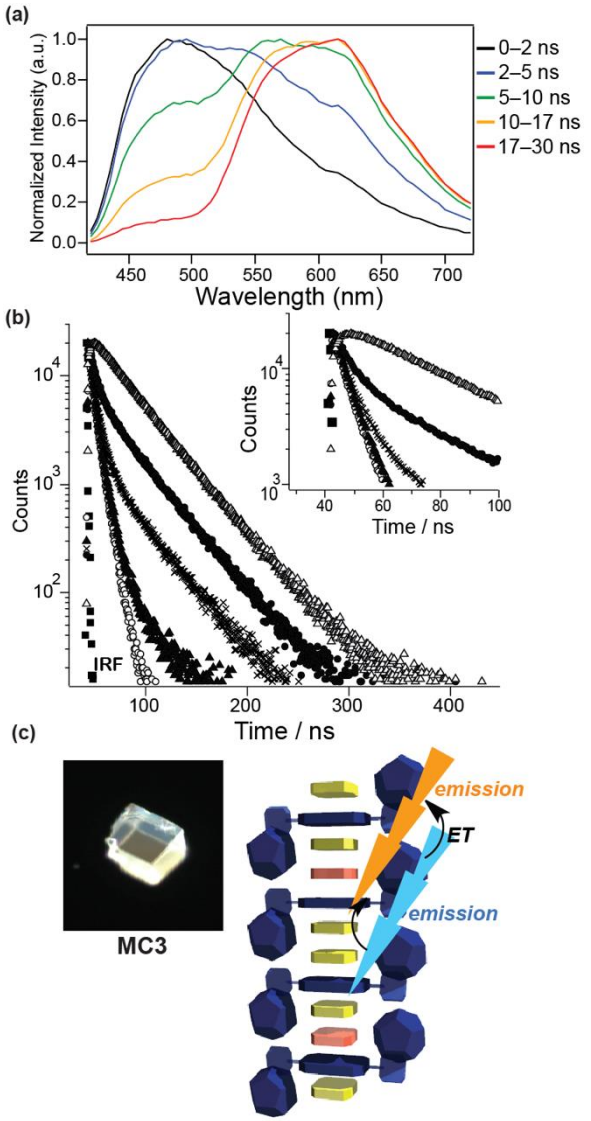

Fig. 5 (a) Time-resolved emission spectra of **MC3** at different times after the pulse (365 nm). Excitation at 365 nm. (b) Emission decay curves of the **MC3** monitored at different wavelength. IRF: ■, 440 nm: ○, 500 nm: ▲, 520 nm: ×, 540 nm: ●, 630 nm: △. Excitation at 365 nm. IRF corresponds to instrument response function. (c) Schematic representation of the energy transfer in **MC3**. Photograph shows fluorescence microscopy images of white-light emission of **MC3**.

Fluorescence Time-Resolved Spectroscopy of Four-component Crystals (MC3)

To investigate the excited states of white-light emitting crystals (**MC3**), we performed further nanosecond time-resolved emission spectra at room temperature using nanosecond time-correlated single photon counting (TCSPC). The corresponding relaxation dynamics were then analyzed at each wavelength to reconstruct the temporal evolution of the emission spectrum [Fig. 5(a)]. As time elapsed, the short wavelength emission bands (420–520 nm) gradually decreased and red-shifted, whereas the long wavelength emission (520–720 nm) continuously increased and reached its maximum intensity at

around 600 nm. The wavelength dependence of the emission decay curves of **MC3** are shown in Fig. 5(b), while pertinent data are listed in Table 3. In the deep blue region at 440 nm, the time resolved fluorescence consisted of two decay components of 4.0 and 8.2 ns, which were faster than those at longer wavelengths (i.e., lower energy). Upon monitoring at 500, 520, and 540 nm, a rise time of ~40.0 ns appeared. At the longest wavelength monitored (630 nm), the overall kinetics could be well fitted by a rise (4.0 ns and 8.2 ns) and a decay (33.0 and 48.0 ns) component, in which the rise of 4.0 and 8.2 ns exactly matched the decay component of the short wavelength at e.g. 500 nm. Such delayed growth (Fig. 5b, inset) strongly suggests that energy transfer from the higher (blue emission) to the lower (orange emission) energy sites occurred. The relatively longer lifetime may arise from CT states. The possible energy transfer process is shown in Fig. 5c. As shown in the schematic, an appropriate distance between the donor and acceptor was reached owing to a trace of naphthalene molecules well-dispersed in the *m*-fluorotoluene/naphthalene binary guest systems.

Discussion

An overview of the multi-component crystals in this series shows remarkable variation in emission, using host–guest chemistry in the crystals. Deep blue and cyan emissions are achieved in **C1**–**C10**. A range of green, yellow-green, orange, or red to NIR broad-emission are achieved in **C11**–**C14**. By varying the guest ratio and combinations, a wide range of optical properties can be achieved as clearly visible from Fig. 4. White-light emissions are achieved in **MC2**–**MC4**. The emission intensity and the color-tuning are realized by utilizing CT interaction, and effective energy transfer in the crystals. The distribution of the components in **MC1–MC14** remains an open question. The evidence thus far is consistent with random dispersions, but small scale segregation or ordering may occur. Moreover, co-crystals can not be prepared in a predictable way in some cases depending on the size and composition ratio of guest molecules (**C15** and **MC15**–**MC17**). However, slight modification of host molecules (NDI or TPFB) should alter the inherent porosity of crystals, which should enable accommodation of other guest molecules and combinations. Recent advances in supramolecular chemistry allow unique micro-/nano-scale structures include DNA assemblies,[72, 73] supramolecular materials,[46] organogels,[74, 75] and inorganic/organic hybrids[76] that realize the high-efficiency emission properties by hybridization of various components. In the same direction, the multi-component crystals are useful platform to provide hybrid solid-state materials with a variety of compositions for novel photofunciton design.

Table 3. Fitting results of TCSPC spectroscopic measurements for **MC3** at room temperature.

λ_{probe} (nm)	Population decay (ns)
440	τ_1: 4.0 (45.2), τ_2: 8.2 (54.8)
500	τ_1: 4.0 (39.0), τ_2: 8.1 (53.6), τ_3: 38.0 (7.5)
520	τ_1: 4.0 (27.9), τ_2: 8.1 (38.5), τ_3: 38.0 (33.5)
540	τ_1: 4.0 (8.0), τ_2: 8.1(15.3), τ_3: 33.0 (58.4) , τ_4: 48.0 (18.3)
630	τ_1: 4.0 (-1.3), τ_2: 8.1 (-0.1), τ_3: 33.0 (80.1) , τ_4: 48.0 (21.3)

Conclusions

In conclusion, we have demonstrated a rational strategy to design three-, four-, and five-component crystals that can be tuned to produce solid-state fluorescence emission from the deep blue-to-NIR region, including white-light under UV light irradiation. Our strategy is based on the idea of confining small aromatic guest molecules in the supramolecular acceptor hosts (NDI–TPFB complexes), which is suggestive of inclusion phenomena of a crystal engineering technique. The unique luminescence color originated from CT interactions between NDI-to-guest molecules as well as effective energy transfers in the crystalline state, which was fully characterized by X-ray diffraction and solid-state optical spectroscopy. Flexible color tuning and white light emissions were achieved in binary/ternary guest mixed systems, indicating that color emissive crystals can be obtained using multicomponent crystalline systems. These multi-assembly systems open up a new design principle for arranging luminescent CT combinations in a host framework and guest recognitions, offering crystallization induced emissive materials with designable functions. To our knowledge, the field of intermolecular CT crystals or salts mostly focused on high conductivity, superconductivity, or organic ferroelectrics properties, [77] [78] and luminescence CT complex is still rare. Although, crystal structure-optical property relationships are difficult to predict, this represents a unique strategy for designing novel photofunctional solid-state systems.

Experimental Section

Materials and Chemicals.

(trifluoromethyl)benzene (**1**), *o*-difluorobenzene (**2**), *m*-difluorobenzene (**3**), *p*-difluorobenzene (**4**), fluorobenzene (**5**), benzene (**6**), *o*-fluorotoluene (**7**), *m*-fluorotoluene (**8**), *p*-fluorotoluene (**9**), toluene (**10**), *m*-xylene (**11**), mesitylene (**12**), *m*-methylanisole (**13**), 1,3-dimethoxybenzene (**14**) and tris(pentafluorophenyl)borane (TPFB) were purchased from Tokyo Chemical Industry Co., Ltd. (Japan). Naphthalene (**15**) was purchased from Kishida Chemical Co., Ltd. (Japan). All of them were used directly without further purification. The NDI was synthesized according to previous reports.[19]

Crystal Growth and Characterization.

Three Component Crystals.

C1, *NDI:TPFB:(trifluoromethyl)benzene (1:2:1) co-crystal.* NDI (50 mg, 1 eq.), TPFB (125 mg, 2.1 eq.) and (trifluoromethyl)benzene (10 g, excess) were mixed in a sample tube. The mixture was heated up to close to the boiling point, then cooled at 4 °C to obtain colorless crystals. Crystal parameters for **C1**: [$C_{67}H_{17}B_2F_{33}N_4O_4$]. Colorless block (0.10 × 0.10 × 0.28 mm). Triclinic, *P-1*, *a* = 13.4427(13), *b* = 14.1320(14), *c* = 15.7877(15) Å, α = 85.810(2), β = 84.834(2), γ = 88.496(2) °, *V* = 2978.5(5) Å^3, Z = 2, *T* = 100 K, ρ_{calc} = 1.773 g cm^{-3}, μ = 0.181 mm^{-1}. Of a total of 31902 reflections that were collected, 10516 were unique. Final R_1 = 0.0492 and wR_2 = 0.1213. GOF = 1.000. CCDC 1473405 contains the supplementary crystallographic data for this paper. These data can be obtained free of charge from The Cambridge Crystallographic Data Centre.

C2, *NDI:TPFB:o-difluorobenzene (1:2:2) co-crystal.* NDI (50 mg, 1 eq.), TPFB (125 mg, 2.1 eq.) and *o*-difluorobenzene (10 g, excess) were mixed in a sample tube. The mixture was heated up to close to the boiling point, then cooled at 4 °C to obtain colorless crystals. Colorless block (0.21 × 0.34 × 0.46 mm). Monoclinic, *P2(1)/c*, *a* = 20.0151(14), *b* = 19.7169(13), *c* = 16.4873(11) Å, α = 90, β = 102.4660(10), γ = 90 °, *V* = 6353.1(7) Å^3, Z = 4, *T* = 100 K, ρ_{calc} = 1.749 g cm^{-3}, μ = 0.177 mm^{-1}. Of a total of 82950 reflections that were collected, 15138 were unique. Final R_1 = 0.0395 and wR_2 = 0.1076. GOF = 0.999. CCDC 1474114 contains the supplementary crystallographic data for this paper. These data can be obtained free of charge from The Cambridge Crystallographic Data Centre.

C3, *NDI:TPFB:m-difluorobenzene (1:2:2) co-crystal.* NDI (50 mg, 1 eq.), TPFB (125 mg, 2.1 eq.) and *m*-difluorobenzene (10 g, excess) were mixed in a sample tube. The mixture was heated up to close to the boiling point, then cooled at 4 °C to obtain colorless crystals. Colorless block (0.13 × 0.16 × 0.61 mm). Monoclinic, *P2(1)/c*, *a* = 19.909(4), *b* = 19.531(4), *c* = 16.642(3) Å, α = 90, β = 100.891(3), γ = 90 °, *V* = 6355.(2) Å^3, Z = 4, *T* = 100 K, ρ_{calc} = 1.748 g cm^{-3}, μ = 0.177 mm^{-1}. Of a total of 59977 reflections that were collected, 10172 were unique. Final R_1 = 0.0500 and wR_2 = 0.1353. GOF = 0.992. CCDC 1474116 contains the supplementary crystallographic data for this paper. These data can be obtained free of charge from The Cambridge Crystallographic Data Centre.

C4, *NDI:TPFB:p-difluorobenzene (1:2:2) co-crystal.* NDI (50 mg, 1 eq.), **TPFB** (125 mg, 2.1 eq.) and *p*-difluorobenzene (10 g, excess) were mixed in a sample tube. The mixture was heated up to close to the boiling point, then cooled at 4 °C to obtain colorless crystals. Colorless block (0.10 × 0.10 × 0.28 mm). Monoclinic, *P2(1)/c*, *a* = 19.7642(14), *b* = 19.9220(14), *c* = 16.6275(12) Å, α = 90, β = 102.3960(10), γ = 90 °, *V* = 6394.3(8) Å^3, Z = 4, *T* = 100 K, ρ_{calc} = 1.737 g cm^{-3}, μ = 0.176 mm^{-1}. Of a total of 71846 reflections that were collected, 12640 were unique. Final R_1 = 0.0432 and wR_2 = 0.1023. GOF = 1.021. CCDC 1474118 contains the supplementary crystallographic data for this paper. These data can be obtained free of charge from The Cambridge Crystallographic Data Centre.

C5, *NDI:TPFB:fluorobenzene (1:2:2) co-crystal.* NDI (50 mg, 1 eq.), **TPFB** (125 mg, 2.1 eq.) and fluorobenzene (10 g, excess) were mixed in a sample tube. The mixture was heated up to close to the boiling point, then cooled at 4 °C to obtain pale yellow crystals. Colorless block (0.18 × 0.25 × 0.50 mm). Monoclinic, *P2(1)/c*, *a* = 19.958(3), *b* = 19.786(3), *c* = 16.513(2) Å, α = 90, β = 102.162(2), γ = 90 °, *V* = 6374.4(14) Å^3, Z = 4, *T* = 100 K, ρ_{calc} = 1.706 g cm^{-3}, μ = 0.170 mm^{-1}. Of a total of 62895 reflections that were collected, 10488 were unique. Final R_1 = 0.0547 and wR_2 = 0.1460. GOF = 1.052. CCDC 1559549 contains the supplementary crystallographic data for this paper. These data can be obtained free of charge from The Cambridge Crystallographic Data Centre.

C6, *NDI:TPFB:benzene (1:2:2) co-crystal.* NDI (50 mg, 1 eq.), TPFB (125 mg, 2.1 eq.) and benzene (10 g, excess) were mixed in a sample tube. The mixture was heated up to close to the boiling point, soon after the pale yellow crystals were precipitated. Colorless block (0.10 × 0.10 × 0.28 mm). Monoclinic, *P2(1)/c*, *a* = 19.915(3), *b* = 19.847(3), *c* = 16.513(3) Å, α = 90, β = 102.719(3), γ = 90 °, *V* = 6366.7(19) Å^3, Z = 4, *T* = 100 K, ρ_{calc} = 1.670 g cm^{-3}, μ = 0.164 mm^{-1}. Of a total of 64135 reflections that were collected, 10739 were unique. Final R_1 = 0.0529 and wR_2 = 0.1211. GOF = 0.994. CCDC 1053318 contains the supplementary crystallographic data for this paper. These data can be obtained free of charge from The Cambridge Crystallographic Data Centre.

C7, *NDI:TPFB:o-fluorotoluene (1:2:2) co-crystal.* NDI (50 mg, 1 eq.), **TPFB** (125 mg, 2.1 eq.) and o-fluorotoluene (10 g, excess) were mixed in a sample tube. The mixture was heated up to close to the boiling point, soon after the pale yellow crystals were precipitated. Colorless block (0.14 × 0.19 × 0.45 mm). Monoclinic, *P2(1)/c*, *a* = 20.0647(16), *b* = 20.4856(16), *c* = 16.4295(13) Å, α = 90, β = 104.9420(10), γ = 90 °, *V* = 6524.8(9) Å^3, Z = 4, *T* = 100 K, ρ_{calc} = 1.695 g cm^{-3}, μ = 0.168 mm^{-1}. Of a total of 88211 reflections that were collected, 16180 were unique. Final R_1 = 0.0545 and wR_2 = 0.1542. GOF = 1.029. CCDC 1474119 contains the supplementary crystallographic data for this paper. These data can be obtained free of charge from The Cambridge Crystallographic Data Centre.

C8, *NDI:TPFB:m-fluorotoluene (1:2:2) co-crystal.* NDI (50 mg, 1 eq.), **TPFB** (125 mg, 2.1 eq.) and *m*-fluotoluene (10 g, excess) were mixed in a sample tube. The mixture was heated up to close to the boiling point, soon after the pale yellow crystals were precipitated. Colorless block (0.10 × 0.18 × 0.26 mm). Monoclinic, *P2(1)/c*, *a* = 20.0295(19), *b* = 20.6089(19), *c* = 16.3863(15) Å, α = 90, β = 105.0920(10), γ = 90 °, *V* = 6530.7(11) Å^3, Z = 4, *T* = 100 K, ρ_{calc} = 1.693 g cm^{-3}, μ = 0.168 mm^{-1}. Of a total of 89224 reflections that were collected, 16627 were unique. Final R_1 = 0.0656 and wR_2 = 0.1709. GOF = 0.998. CCDC 1053321 contains the supplementary crystallographic data for this paper. These data can be obtained free of charge from The Cambridge Crystallographic Data Centre.

C9, *NDI:TPFB:p-fluorotoluene (1:2:2) co-crystal.* NDI (50 mg, 1 eq.), **TPFB** (125 mg, 2.1 eq.) and *p*-fluotoluene (10 g, excess) were mixed in a sample tube. The mixture was heated up to close to the boiling point, soon after the pale yellow crystals were precipitated. Pale yellow block (0.23 × 0.35 × 0.40 mm). Monoclinic, *P2(1)/c*, *a* = 20.1002(13), *b* = 20.5714(14), *c* = 16.2701(11) Å, α = 90, β = 105.0990(10), γ = 90 °, *V* = 6495.3(8) Å^3, Z = 4, *T* = 100 K, ρ_{calc} = 1.702 g cm^{-3}, μ = 0.169 mm^{-1}. Of a

total of 92038 reflections that were collected, 17653 were unique. Final R_1 = 0.0425 and wR_2 = 0.1177. GOF = 0.989. CCDC 1474120 contains the supplementary crystallographic data for this paper. These data can be obtained free of charge from The Cambridge Crystallographic Data Centre.

C10, *NDI:TPFB:toluene (1:2:2) co-crystal.* NDI (50 mg, 1 eq.), TPFB (125 mg, 2.1 eq.) and toluene (10 g, excess) were mixed in a sample tube. The mixture was heated up to close to the boiling point, soon after the yellow crystals were precipitated. Yellow block (0.17 × 0.25 × 0.76 mm). Monoclinic, *P2(1)/c*, *a* = 20.0230(14), *b* = 20.3398(14), *c* = 16.3764(11) Å, α = 90, β = 104.4960(10), γ= 90 °, *V* = 6457.2(8) Å^3, Z = 4, *T* = 100 K, ρ_{calc}= 1.655 g cm^{-3}, μ = 0.161 mm^{-1}. Of a total of 93764 reflections that were collected, 18736 were unique. Final R_1 = 0.0488 and wR_2 = 0.1169. GOF = 0.974. CCDC 1053322 contains the supplementary crystallographic data for this paper. These data can be obtained free of charge from The Cambridge Crystallographic Data Centre.

C11, *NDI:TPFB:m-xylene (1:2:2) co-crystal.* NDI (50 mg, 1 eq.), TPFB (125 mg, 2.1 eq.) and *m*-xylene (10 g, excess) were mixed in a sample tube. The mixture was heated up to close to the boiling point, soon after the yellow crystals were precipitated. Yellow block (0.18 × 0.20 × 0.38 mm). Monoclinic, *P2(1)/n*, *a* = 11.374(2), *b* = 20.799(4), *c* = 14.400(3) Å, α = 90, β = 99.032(3), γ= 90 °, *V* = 3364.3(11) Å^3, Z = 2, *T* = 100 K, ρ_{calc}= 1.635 g cm^{-3}, μ = 0.158 mm^{-1}. Of a total of 46011 reflections that were collected, 8539 were unique. Final R_1 = 0.0539 and wR_2 = 0.1123. GOF = 1.035. CCDC 1053323 contains the supplementary crystallographic data for this paper. These data can be obtained free of charge from The Cambridge Crystallographic Data Centre.

C12, *NDI:TPFB:1,3,5-trimethylbenzene (1:2:2) Cocrystal.* NDI (50 mg, 1 eq.), TPFB (125 mg, 2.1 eq.) and 1,3,5-trimethylbenzene (10 g, excess) were mixed in a sample tube. The mixture was heated up to close to the boiling point, soon after the yellow crystals were precipitated. Yellow block (0.14 × 0.18 × 0.40 mm). Monoclinic, *P2(1)/n*, *a* = 11.1604(11), *b* = 21.035(2), *c* = 14.8978(15) Å, α = 90, β = 99.764(2), γ= 90 °, *V* = 3446.7(6) Å^3, Z = 2, *T* = 100 K, ρ_{calc}= 1.623 g cm^{-3}, μ = 0.156 mm^{-1}. Of a total of 40997 reflections that were collected, 7108 were unique. Final R_1 = 0.0398 and wR_2 = 0.1075. GOF = 1.024. CCDC 1053324 contains the supplementary crystallographic data for this paper. These data can be obtained free of charge from The Cambridge Crystallographic Data Centre.

C13, *NDI:TPFB:m-methylanisole (1:2:2) co-crystal.* NDI (50 mg, 1 eq.), TPFB (125 mg, 2.1 eq.) and *m*-methylanisole (10 g, excess) were mixed in a sample tube. The mixture was heated up to close to the boiling point, soon after the orange crystals were precipitated. Orange block (0.10 × 0.15 × 0.44 mm). Monoclinic, *P2(1)/n*, *a* = 11.4404(9), *b* = 20.9135(16), *c* = 14.3076(11) Å, α = 90, β= 99.7200(10), γ= 90 °, *V* = 3374.1(5) Å^3, Z = 2, *T* = 100 K, ρ_{calc}= 1.662 g cm^{-3}, μ = 0.162 mm^{-1}. Of a total of 47201 reflections that were collected, 8726 were unique. Final R_1 = 0.0441 and wR_2 = 0.1140. GOF = 1.003. CCDC 1053325 contains the supplementary crystallographic data for this paper. These data can be obtained free of charge from The Cambridge Crystallographic Data Centre.

C14, *NDI:TPFB:1,3,-dimethoxybenzene* (1:2:2) *co-crystal*. **NDI** (50 mg, 1 eq.), TPFB (125 mg, 2.1 eq.) and *m*-methylanisole (10 g, excess) were mixed in a sample tube. The mixture was heated up to close to the boiling point, soon after the orange crystals were precipitated. Orange block (0.20 × 0.20 × 0.25 mm). Monoclinic, *P2(1)/n*, *a* = 11.269(8), *b* = 21.529(15), *c* = 14.2601(10) Å, α = 90, β = 95.458(8), γ= 90 °, *V* = 3444.(4) Å^3, Z = 2, *T* = 100 K, ρ_{calc}= 1.659 g cm^{-3}, μ = 0.162 mm^{-1}. Of a total of 24187 reflections that were collected, 8854 were unique. Final R_1 = 0.0449 and wR_2 = 0.1539. GOF = 0.941. CCDC 1474122 contains the supplementary crystallographic data for this paper. These data can be obtained free of charge from The Cambridge Crystallographic Data Centre.

4-2-2. Four- and Five-component Crystals.

MC1, *NDI:TPFB:m-fluorotoluene:naphthalene (1:2:1.956:0.044) co-crystal.* NDI (100 mg, 1 eq.), TPFB (250 mg, 2.1 eq.), *m*-fluorobenzene (19.5 g) and naphthalene (0.5 g) were mixed in a sample tube. The mixture was heated up to close to the boiling point, soon after the pale yellow crystals were precipitated. Molar ratio of guest molecules was determined by ^{1}H-NMR measurement.

MC2, *NDI:TPFB:m-fluorotoluene:naphthalene (1:2:1.940:0.060) co-crystal.* NDI (100 mg, 1 eq.), TPFB (250 mg, 2.1 eq.), *m*-fluorobenzene (19.0 g) and naphthalene (1.0 g) were mixed in a sample tube. The mixture was heated up to close to the boiling point, soon after the pale yellow crystals were precipitated. Molar ratio of guest molecules was determined by ^{1}H-NMR measurement.

MC3, *NDI:TPFB:m-fluorotoluene:naphthalene (1:2:1.934:0.066) Cocrystal.* NDI (100 mg, 1 eq.), TPFB (250 mg, 2.1 eq.), *m*-fluorobenzene (18.5 g) and naphthalene (1.5 g) were mixed in a sample tube. The mixture was heated up to close to the boiling point, soon after the pale yellow crystals were precipitated. Molar ratio of guest molecules was determined by ^{1}H-NMR measurement.

MC4, *NDI:TPFB:m-fluorotoluene:naphthalene (1:2:1.906:0.094) co-crystal.* NDI (100 mg, 1 eq.), TPFB (250 mg, 2.1 eq.), *m*-fluorobenzene (15.0 g) and naphthalene (5.0 g) were mixed in a sample tube. The mixture was heated up to close to the boiling point, soon after the pale yellow crystals were precipitated. Molar ratio of guest molecules was determined by ^{1}H-NMR measurement.

MC5, *NDI:TPFB:m-fluorotoluene:naphthalene (1:2:1.828:0.172) co-crystal.* NDI (100 mg, 1 eq.), TPFB (250 mg, 2.1 eq.), *m*-fluorobenzene (19.5 g) and naphthalene (0.5 g) were mixed in a sample tube. The mixture was heated up to close to the boiling point, soon after the pale yellow crystals were precipitated. Molar ratio of guest molecules was determined by ^{1}H-NMR measurement.

MC6, *NDI:TPFB:toluene:naphthalene (1:2:1.870:0.130) co-crystal.* **NDI** (100 mg, 1 eq.), TPFB (250 mg, 2.1 eq.), toluene (19.5 g) and naphthalene (0.5 g) were mixed in a sample tube. The mixture was heated up to close to the boiling point, soon after the pale yellow crystals were precipitated. Molar ratio of guest molecules was determined by ^{1}H-NMR measurement.

MC7, *NDI:TPFB:toluene:naphthalene (1:2:1.840:0.160) co-crystal.* NDI (100 mg, 1 eq.), TPFB (250 mg, 2.1 eq.), toluene

(19.5 g) and naphthalene (0.5 g) were mixed in a sample tube. The mixture was heated up to close to the boiling point, soon after the pale yellow crystals were precipitated. Molar ratio of guest molecules was determined by ^{1}H-NMR measurement.

MC8, *NDI:TPFB:toluene:naphthalene (1:2:1.816:0.184) Cocrystal.* NDI (100 mg, 1 eq.), TPFB (250 mg, 2.1 eq.), toluene (19.5 g) and naphthalene (0.5 g) were mixed in a sample tube. The mixture was heated up to close to the boiling point, soon after the pale yellow crystals were precipitated. Molar ratio of guest molecules was determined by ^{1}H-NMR measurement.

MC9, *NDI:TPFB:m-xylene:naphthalene (1:2:1.896:0.104) co-crystal.* NDI (100 mg, 1 eq.), TPFB (250 mg, 2.1 eq.), *m*-xylene (19.5 g) and naphthalene (0.5 g) were mixed in a sample tube. The mixture was heated up to close to the boiling point, soon after the pale yellow crystals were precipitated. Molar ratio of guest molecules was determined by ^{1}H-NMR measurement.

MC10, *NDI:TPFB:m-xylene:naphthalene (1:2:1.878:0.122) co-crystal.* NDI (100 mg, 1 eq.), TPFB (250 mg, 2.1 eq.), *m*-xylene (19.5 g) and naphthalene (0.5 g) were mixed in a sample tube. The mixture was heated up to close to the boiling point, soon after the pale yellow crystals were precipitated. Molar ratio of guest molecules was determined by ^{1}H-NMR measurement.

MC11, *NDI:TPFB:m-xylene:naphthalene (1:2:1.816:0.184) co-crystal.* NDI (100 mg, 1 eq.), TPFB (250 mg, 2.1 eq.), *m*-xylene (19.5 g) and naphthalene (0.5 g) were mixed in a sample tube. The mixture was heated up to close to the boiling point, soon after the pale yellow crystals were precipitated. Molar ratio of guest molecules was determined by ^{1}H-NMR measurement.

MC12, *NDI:TPFB:m-fluorotoluene:m-xylene:naphthalene (1:2:1.784:0.182:0.034) co-crystal.* NDI (100 mg, 1 eq.), TPFB (250 mg, 2.1 eq.), *m*-fluorobenzene (18.0 g), *m*-fluorobenzene (2.0 g), and naphthalene (0.5 g) were mixed in a sample tube. The mixture was heated up to close to the boiling point, soon after the pale yellow crystals were precipitated. Molar ratio of guest molecules was determined by ^{1}H-NMR measurement.

MC13, *NDI:TPFB:m-fluorotoluene:m-xylene:naphthalene (1:2:1.726:0.250:0.042) co-crystal.* NDI (100 mg, 1 eq.), TPFB (250 mg, 2.1 eq.), *m*-fluorobenzene (18.0 g), *m*-xylene (1.0 g) and naphthalene (1.0 g) were mixed in a sample tube. The mixture was heated up to close to the boiling point, soon after the pale yellow crystals were precipitated. Molar ratio of guest molecules was determined by ^{1}H-NMR measurement.

MC14, *NDI:TPFB:m-fluorotoluene:m-xylene:naphthalene (1:2:1.620:0.290:0.090) co-crystal.* NDI (100 mg, 1 eq.), TPFB (250 mg, 2.1 eq.), *m*-fluorobenzene (17.0 g), *m*-xylene (1.0 g) and naphthalene (2.0 g) were mixed in a sample tube. The mixture was heated up to close to the boiling point, soon after the pale yellow crystals were precipitated. Molar ratio of guest molecules was determined by ^{1}H-NMR measurement.

MC15, *NDI:TPFB:m-fluorotoluene:m-methylanisole (1:2:1.800:0.200) co-crystal.* NDI (100 mg, 1 eq.), TPFB (250 mg, 2.1 eq.), *m*-fluorobenzene (19.5 g) and naphthalene (0.5 g) were mixed in a sample tube. The mixture was heated up to close to the boiling point, soon after the pale yellow crystals were precipitated. Molar ratio of guest molecules was determined by ^{1}H-NMR measurement.

MC16, *NDI:TPFB:m-fluorotoluene:m-methylanisole (1:2:1.560:0.440) co-crystal.* NDI (100 mg, 1 eq.), TPFB (250 mg, 2.1 eq.), *m*-fluorobenzene (19.0 g) and *m-methylanisole* (1.0 g) were mixed in a sample tube. The mixture was heated up to close to the boiling point, soon after the pale yellow crystals were precipitated. Molar ratio of guest molecules was determined by ^{1}H-NMR measurement.

MC17, *NDI:TPFB:m-fluorotoluene:m-methylanisole (1:2:1.400: 0.600) co-crystal.* NDI (100 mg, 1 eq.), TPFB (250 mg, 2.1 eq.), *m*-fluorobenzene (18.0 g) and *m-methylanisole* (2.0 g) were mixed in a sample tube. The mixture was heated up to close to the boiling point, soon after the pale yellow crystals were precipitated. Molar ratio of guest molecules was determined by ^{1}H-NMR measurement.

Characterization

PXRD data were collected using a Rigaku SmartLab system (Rigaku) diffractometer with a copper K-alpha source. The crystals that were used for the PXRD measurement were gently ground by agate mortar and pestle. The simulated patterns were obtained from single-crystal X-ray analysis. ^{1}H NMR spectra were recorded on a Bruker AV300 NMR spectrometer (300 MHz) and Bruker AVANCE-500K-S NMR spectrometer (500 MHz). Tetramethylsilane (TMS) was used as an internal standard (0 ppm). The TGA measurements were carried out using a TG/DTA7300 system (Seiko Instruments Inc.) in the temperature range of 303-773 K under flowing N_2 gas at a heating rate of 10 K min^{-1}.

X-ray crystal structural analysis.

The crystals were mounted on a loop. Diffraction data for the crystal samples was collected at 100 K on a Bruker SMART APEX CCD detector with graphite-monochromated Mo $K\alpha$ radiation (λ = 0.71073 Å). From the collected data, unit cell, integration, absorption correction, and space group were determined using the Bruker APEX3 software package.[79] The data frames were integrated using SAINT and merged to give a unique data set for the structure determination. Empirical absorption corrections by SADABS were carried out. Hydrogen atoms were located at calculated positions and included in the structure factor calculation but were not refined. Crystallographic data have been deposited with the Cambridge Crystallographic Data Centre. The data can be obtained free of charge on application to CCDC, 12 Union Road, Cambridge CB21EZ, UK (fax: (+44) 1223-336-033; email: deposit@ccdc.cam.ac.uk).

Optical Characterization

UV-vis diffuse reflectance measurements were recorded using a JASCO V-670 spectrometer (JASCO) with an integration sphere attachment. Fluorescence excitation and emission spectra were collected at room temperature on a Hitachi F-7000 fluorescence spectrometer. Emission spectra were collected in the range between 380-720 nm, with a scan speed of 240 nm/min, and the slits were set at 5.0 nm (excitation slit) and 5.0 nm (emission slit) unless otherwise noted. The excitation wavelength is 370 nm. The absolute photoluminescence quantum yields (Φ_{PL}) were determined as a solid state using

absolute PL quantum yields measurement system C9920-02 (Hamamatsu photonics) after excitation at 370 nm. Time-resolved photoluminescence lifetimes were curried out by using time-correlated single photon counting lifetime spectroscopy system, Quantaurus-Tau C11367-02 (Hamamatsu photonics). The decay constants and fitting parameters (τ_1, τ_2, τ_3, τ_4, A_1, A_2, A_3, A_4) for transient decays were determined using the embedded software of Quantaurus-Tau. For the time-resolved spectroscopy, the emission decay curves were recorded as a function of the emission wavelength in the 420–720 nm range (the wavelength increment was 5 nm) for a fixed recording time (200 s per wavelength). The emission spectra at different times after excitation were obtained by averaging the integrated emission intensity for different time windows at every wavelength after the excitation pulse. Fluorescence images were visualized under fluorescence microscope (Carl Zeiss Axio Imager.A2). The excitation source was a xenon lamp equipped with a band-pass filter (330–380 nm).

Conflicts of interest

There are no conflicts to declare.

Acknowledgements

This work was supported by JST PRESTO Grant Number JPMJPR1414 and by JSPS KAKENHI Grant Numbers JP17H04875 (Grant-in-Aid for Young Scientists (A) for T. O.), JP17H05161 (π-System Figuration for T. O.), JP16H04119 (Grant-in-Aid for Scientific Research (B) for Y. H.), JP18H04265 (Precisely Designed Catalysts with Customized Scaffolding for Y. H.), Tonen General Sekiyu Foundation, Shitagau Noguchi Foundation, and Nissan Chemical Corporation. We thank Prof. N. Nakashima and T. Fujigaya for the use of PXRD measurements, Ms. A. Goto for the assistance of optical measurements.

Notes and references

1 J. W. Steed, Trends *Pharmacol. Sci.*, 2013, **34**, 185-193.
2 D. Yan and D. G. Evans, *Mater. Horiz.*, 2014, **1**, 46-57.
3 S. Varughese, *J. Mater. Chem. C*, 2014, **2**, 3499-3516.
4 L. Sun, W. Zhu, F. Yang, B. Li, X. Ren, X. Zhang and W. Hu, *Phys. Chem. Chem. Phys.*, 2018, **20**, 6009-6023.
5 M. Lusi, *Cryst. Growth Des.*, 2018, **18**, 3704-3712.
6 Y. Chujo and K. Tanaka, *Bull. Chem. Soc. Jpn.*, 2015, **88**, 633-643.
7 D. Yan, *Chem. Eur. J.*, 2015, **21**, 4880-4896.
8 D. Yan, A. Delori, G. O. Lloyd, T. Friscic, G. M. Day, W. Jones, J. Lu, M. Wei, D. G. Evans and X. Duan, *Angew. Chem. Int. Ed.*, 2011, **50**, 12483-12486.
9 O. Bolton, K. Lee, H. J. Kim, K. Y. Lin and J. Kim, *Nat. Chem.*, 2011, **3**, 205-210.
10 T. Hinoue, M. Miyata, I. Hisaki and N. Tohnai, *Angew. Chem. Int. Ed.*, 2012, **51**, 155-158.
11 D. Yan, H. Yang, Q. Meng, H. Lin and M. Wei, *Adv. Func. Mater.*, 2014, **24**, 587-594.
12 W. Zhu, R. Zheng, Y. Zhen, Z. Yu, H. Dong, H. Fu, Q. Shi and W. Hu, *J. Am. Chem. Soc.*, 2015, **137**, 11038-11046.
13 Y. Kita, J. Nishida, S. Nishida, Y. Matsui, H. Ikeda, Y. Hirao and T. Kawase, *Chemphotochem*, 2018, **2**, 42-52.
14 Y. L. Lei, Y. Jin, D. Y. Zhou, W. Gu, X. B. Shi, L. S. Liao and S. T. Lee, *Adv. Mater.*, 2012, **24**, 5345-5351.
15 Y.-Q. Sun, Y.-L. Lei, X.-H. Sun, S.-T. Lee and L.-S. Liao, *Chem. Mater.*, 2015, **27**, 1157-1163.
16 L. Sun, W. Zhu, W. Wang, F. Yang, C. Zhang, S. Wang, X. Zhang, R. Li, H. Dong and W. Hu, *Angew. Chem. Int. Ed.*, 2017, **56**, 7831-7835.
17 Y. Sun, Y. Lei, L. Liao and W. Hu, *Angew. Chem. Int. Ed.,* 2017, **56**, 10352-10356.
18 S. Ohtani, M. Gon, K. Tanaka and Y. Chujo, *Chem. Eur. J.*, 2017, **23**, 11827-11833.
19 T. Ono, M. Sugimoto and Y. Hisaeda, *J. Am. Chem. Soc.*, 2015, **137**, 9519-9522.
20 T. Ono, A. Taema, A. Goto and Y. Hisaeda, *Chem. Eur. J.*, 2018, **24**, 17487-17596.
21 G. R. Desiraju, *Angew. Chem. Int. Ed.*, 1995, **34**, 2311-2327.
22 J. D. Wuest, *Chem. Commun.*, 2005, 5830-5837.
23 G. R. Desiraju, *J. Am. Chem. Soc.*, 2013, **135**, 9952-9967.
24 H. Jiang, P. Hu, J. Ye, K. K. Zhang, Y. Long, W. Hu and C. Kloc, *J. Mater. Chem. C*, 2018, **6**, 1884-1902.
25 R. Bishop, *Chem. Soc. Rev.*, 1996, 25, 311-319.
26 A. Das and S. Ghosh, *Angew. Chem. Int. Ed.*, 2014, **53**, 2038-2054.
27 M. Morimoto, S. Kobatake and M. Irie, *J. Am. Chem. Soc.*, 2003, **125**, 11080-11087.
28 K. Sada, K. Inoue, T. Tanaka, A. Epergyes, A. Tanaka, N. Tohnai, A. Matsumoto and M. Miyata, *Angew. Chem. Int. Ed.*, 2005, **44**, 7059-7062.
29 T. Tani, Y. Goto, K. Nonaka, S. Shinkai and K. Sada, *Chem. Lett.*, 2011, 40, 273-275.
30 M. Dabros, P. R. Emery and V. R. Thalladi, *Angew. Chem. Int. Ed.*, 2007, **46**, 4132-4135.
31 S. Tothadi, A. Mukherjee and G. R. Desiraju, *Chem. Commun.*, 2011, **47**, 12080-12082.
32 R. Natarajan, G. Magro, L. N. Bridgland, A. Sirikulkajorn, S. Narayanan, L. E. Ryan, M. F. Haddow, A. G. Orpen, J. P. H. Charmant, A. J. Hudson and A. P. Davis, *Angew. Chem. Int. Ed.*, 2011, **50**, 11386-11390.
33 L. Travaglini, L. N. Bridgland and A. P. Davis, *Chem. Commun.*, 2014, **50**, 4803-4805.
34 T. Hasell, S. Y. Chong, M. Schmidtmann, D. J. Adams and A. I. Cooper, *Angew. Chem. Int. Ed.*, 2012, **51**, 7154-7157.
35 M. Paul, S. Chakraborty and G. R. Desiraju, *J. Am. Chem. Soc.*, 2018, **140**, 2309-2315.
36 T. Ogawa, M. Hosoyamada, B. Yurash, T.-Q. Nguyen, N. Yanai and N. Kimizuka, *J. Am. Chem. Soc.*, 2018, **140**, 8788-8796.
37 H. X. Deng, C. J. Doonan, H. Furukawa, R. B. Ferreira, J. Towne, C. B. Knobler, B. Wang and O. M. Yaghi, *Science*, 2010, **327**, 846-850.
38 T. Fukushima, S. Horike, Y. Inubushi, K. Nakagawa, Y. Kubota, M. Takata and S. Kitagawa, *Angew. Chem. Int. Ed.*, 2010, **49**, 4820-4824.
39 R. Sola-Llano, V. Martínez-Martínez, S. Furukawa, Y. Takashima and I. López-Arbeloa, *Polymers*, 2018, **10**, 188.
40 J. D. Wuest, *Nat. Chem.*, 2012, **4**, 74-75.
41 J. Mei, N. L. C. Leung, R. T. K. Kwok, J. W. Y. Lam and B. Z. Tang, *Chem. Rev.*, 2015, **115**, 11718-11940.
42 D. Li, J. Wang and X. Ma, *Adv. Opt. Mater.*, 2018, **6**, 1800273.
43 S. Mukherjee and P. Thilagar, *Dyes Pigm.*, 2014, **110**, 2-27.
44 C. Vijayakumar, K. Sugiyasu and M. Takeuchi, *Chem. Sci.*, 2011, **2**, 291-294.
45 S. Santhosh Babu, J. Aimi, H. Ozawa, N. Shirahata, A. Saeki, S. Seki, A. Ajayaghosh, H. Mohwald and T. Nakanishi, *Angew. Chem. Int. Ed.*, 2012, **51**, 3391-3395.

46 R. Abbel, C. Grenier, M. J. Pouderoijen, J. W. Stouwdam, P. E. L. G. Leclère, R. P. Sijbesma, E. W. Meijer and A. P. H. J. Schenning, *J. Am. Chem. Soc.*, 2009, **131**, 833-843.
47 X. Zhang, S. Rehm, M. M. Safont-Sempere and F. Würthner, *Nat. Chem.*, 2009, **1**, 623.
48 F. Gai, T. Zhou, L. Zhang, X. Li, W. Hou, X. Yang, Y. Li, X. Zhao, D. Xu, Y. Liu and Q. Huo, *Nanoscale*, 2012, **4**, 6041-6049.
49 F. Li, C. Li, X. Liu, Y. Chen, T. Bai, L. Wang, Z. Shi and S. Feng, *Chem. Eur. J.*, 2012, **18**, 11641-11646.
50 R. Nishiyabu, Y. Sugino and Y. Kubo, *Chem. Commun.*, 2013, **49**, 9869-9871.
51 S. V. Bhosale, C. H. Jani and S. J. Langford, *Chem. Soc. Rev.*, 2008, **37**, 331-342.
52 M. A. Kobaisi, S. V. Bhosale, K. Latham, A. M. Raynor and S. V. Bhosale, *Chem. Rev.*, 2016, **116**, 11685-11796.
53 S.-L. Suraru and F. Würthner, *Angew. Chem. Int. Ed.*, 2014, **53**, 7428-7448.
54 J.-Z. Liao, L. Meng, J.-H. Jia, D. Liang, X.-L. Chen, R.-M. Yu, X.-F. Kuang and C.-Z. Lu, *Chem. Eur. J.*, 2018, **24**, 10498-10502.
55 S. Bartocci, J. A. Berrocal, P. Guarracino, M. Grillaud, L. Franco and M. Mba, *Chem. Eur. J.*, 2018, **24**, 2920-2928.
56 D. M. Răsădean, B. Sheng, J. Dash and G. D. Pantoş, *Chem. Eur. J.*, 2017, **23**, 8491-8499.
57 A. Takai, T. Kajitani, T. Fukushima, K. Kishikawa, T. Yasuda and M. Takeuchi, *J. Am. Chem. Soc.*, 2016, **138**, 11245-11253.
58 Y. Wu, M. D. Krzyaniak, J. F. Stoddart and M. R. Wasielewski, *J. Am. Chem. Soc.*, 2017, **139**, 2948-2951.
59 54. J.-J. Liu, T. Liu, S.-B. Xia, C.-X. He, F.-X. Cheng, M.-J. Lin and C.-C. Huang, *Dyes Pigm.*, 2018, **149**, 59-64.
60 55. A.-B. Bornhof, A. Bauzá, A. Aster, M. Pupier, A. Frontera, E. Vauthey, N. Sakai and S. Matile, *J. Am. Chem. Soc.*, 2018, **140**, 4884-4892.
61 Y. Zhao, Y. Cotelle, L. Liu, J. López-Andarias, A.-B. Bornhof, M. Akamatsu, N. Sakai and S. Matile, *Acc. Chem. Res.*, 2018, **51**, 2255-2263.
62 S. Hatanaka, T. Ono and Y. Hisaeda, *Chem. Eur. J.*, 2016, **22**, 10346-10350.
63 T. Ono, Y. Tsukiyama, A. Taema, H. Sato, H. Kiyooka, Y. Yamaguchi, A. Nagahashi, M. Nishiyama, Y. Akahama, Y. Ozawa, M. Abe and Y. Hisaeda, *ChemPhotoChem*, 2018, **2**, 416-420.
64 J.-J. Liu, Y.-B. Shan, C.-R. Fan, M.-J. Lin, C.-C. Huang and W.-X. Dai, *Inorg. Chem.*, 2016, **55**, 3680-3684.
65 F. Focante, P. Mercandelli, A. Sironi and L. Resconi, *Coord. Chem. Rev.*, 2006, **250**, 170-188.
66 V. R. Thalladi, H.-C. Weiss, D. Bläser, R. Boese, A. Nangia and G. R. Desiraju, *J. Am. Chem. Soc.*, 1998, **120**, 8702-8710.
67 G. R. Desiraju, *Chem. Commun.*, 2005, 2995-3001.
68 C. Kulkarni, G. Periyasamy, S. Balasubramanian and S. J. George, *Phys. Chem. Chem. Phys.*, 2014, **16**, 14661-14664.
69 Y. Takashima, V. M. Martinez, S. Furukawa, M. Kondo, S. Shimomura, H. Uehara, M. Nakahama, K. Sugimoto and S. Kitagawa, *Nat. Commun.*, 2011, **2**, 168.
70 I. E. E. in N. C. W. S.G. Lias, NIST Standard Reference Database Number 69, Eds. P.J. Linstrom and W.G. Mallard, National Institute of Standards and Technology, Gaithersburg MD, 20899, doi:10.18434/T4D303, (retrieved September 3, 2018).
71 E. M. Voigt and C. Reid, *J. Am. Chem. Soc.*, 1964, **86**, 3930-3934.
72 Y. N. Teo, J. N. Wilson and E. T. Kool, *J. Am. Chem. Soc.*, 2009, **131**, 3923-3933.
73 Y. N. Teo and E. T. Kool, *Chem. Rev.*, 2012, **112**, 4221-4245.
74 A. Dawn, T. Shiraki, S. Haraguchi, S.-i. Tamaru and S. Shinkai *Chem. Asian J.*, 2011, **6**, 266-282.
75 R. G. Weiss, *J. Am. Chem. Soc.*, 2014, **136**, 7519-7530.
76 M. Gon, K. Tanaka and Y. Chujo, *Bull. Chem. Soc. Jpn.*, 2017, **90**, 463-474.
77 J. Zhang, W. Xu, P. Sheng, G. Zhao and D. Zhu, *Acc. Chem. Res.*, 2017, **50**, 1654-1662.
78 A. S. Tayi, A. K. Shveyd, A. C. Sue, J. M. Szarko, B. S. Rolczynski, D. Cao, T. J. Kennedy, A. A. Sarjeant, C. L. Stern, W. F. Paxton, W. Wu, S. K. Dey, A. C. Fahrenbach, J. R. Guest, H. Mohseni, L. X. Chen, K. L. Wang, J. F. Stoddart and S. I. Stupp, *Nature*, 2012, **488**, 485-489.
79 A. Bruker, SAINT and SADABS. Bulker AXS Inc., Madison, Wisconsin, USA. 2016.

A series of multi-color and white-light photoluminescence host/guest co-crystals were prepared by cooperative multi-molecular assemblies.